Optical and Quantum Electronics (2024) 56:466
https://doi.org/10.1007/s11082-023-06050-7

Zn^{2+} ion doping's impact on the vibration spectroscopic properties of higher absorption ions: application to the determination of optical constant properties: advancements in nanotechnology applications

Sadiq H. Khoreem[1] · A. H. AL-Hammadi[2] · Azmi A. M. Othman[3]

Received: 27 September 2023 / Accepted: 5 December 2023 / Published online: 27 January 2024

Abstract
The doping of Zn^{2+} ions and their effect on the vibrational spectroscopic characteristics of ions with higher absorption capacity were investigated in this study. The powder X-ray diffraction studies confirmed the formation of W-type hexaferrite structure. XRD results were used to determine the crystallite size and lattice constants of the prepared powders. The average crystallite size was found in the range of 35–37 nm and increased with increase in Zn^{2+} content. The optical properties of $BaNi_{2-x}Zn_xFe_{16}O_{27}$ ferrite were determined using infrared spectra within the 400–4000 cm^{-1} frequency range. The ferrites mentioned in this section were prepared using a conventional double-sintering ceramic technique. During the analysis, two distinct bands were identified in the spectra. The first band, referred to as the high-frequency vibration band ν_1, appeared at approximately 589 cm^{-1}. This band is attributed to vibrations occurring at tetrahedral sites within the spinel lattice structure. The second band, known as the low-frequency band ν_2, was observed between 440 and 448 cm^{-1} which it was assigned to the vibrations occurring at the octahedral locations of the hexagonal lattice. The refractive index, absorption coefficient, and reflectance spectra of the doped ferrites were calculated for different levels of Zn doping. The results demonstrated that the optical characteristics of the material changed because of the addition of zinc ions, including an increase in its absorption capacity, decrease in its reflectance, and changes in its refractive index. These findings provide valuable insights into the characteristics of ferrites as a result of dopants and demonstrate the potential of infrared transformation as a powerful tool for analyzing the optical characteristics of doped magnetic materials. The threshold frequency, denoted as ν_{th}, was determined to analyze the electronic transitions of the system. As the concentration of Zn ions increased, there was an observed rise in the value of ν_{th}. By examining the Fourier transform infrared (FT-IR) spectra, the cation distribution within the mixed ferrite was inferred by examining the FT-IR spectra. The cation distribution was established by correlating the ionic radii associated with each site in the ferrite structure. The application of this research lies in the determination of optical constant properties, with a focus on advancements in nanotechnology. Zn^{2+} ion doping has been found to significantly influence the vibrational spectroscopy of higher absorption ions, leading to observable changes in their optical properties. This study provides valuable insights into the optical properties of doped systems that can be used in various

Extended author information available on the last page of the article

nanotechnology applications. These findings contribute to the development of novel materials with tailored optical properties, enabling advancements in fields such as optoelectronics, photonics, and sensors.

Keywords Nanoferrites · Infrared spectroscopy · Threshold frequency · Optical parameters · Cation distribution

1 Introduction

Ferrite nanoparticles have attracted considerable interest because of their improved electromagnetic and extraordinary physical properties. Moisture content sensors, recording storage devices, microwave products, catalysts, storage of information, electromagnetic resonance imaging, ceramic coverings for solar energy cells, semiconductors, and electronic devices are just a few examples of the many uses of W-type hexaferrites in science, business, and technology. However, in recent years, an interest to utilize the magnetic materials for magneto-optical applications is emerged (Ramzan et al. 2019). The field of nanotechnology has witnessed remarkable progress in the development of functional materials with tailored optical properties. Doping, which involves the intentional introduction of impurity ions into host materials, offers a powerful approach to modulate and optimize the optical and electronic functionalities of nanomaterials. This literature review aims to provide a comprehensive overview of the research conducted on the impact of Zn^{2+} ion doping on the vibration spectroscopy of higher absorption ions in $BaNi_{2-x}Zn_xFe_{16}O_{27}$, and its application in determining optical constant properties. The advancements made in this area hold significant promise for nanotechnology applications (Dhiman et al. 2021; Bharati et al. 2020; Kulkarni and Mathad 2021). Dielectric materials have gained attention for their significant transmission capabilities in the optical spectrum compared with other material categories. Hence, in order to comprehend the optical properties of ferrite materials, it becomes imperative to compute optical characteristics such as absorption, transmission, reflection, and refractive index values (Narang and Pubby 2021).

A study was conducted on Ni–Zn ferrites, where the substitution of Zn^{2+} ions favored tetrahedral locations, whereas customized magnetic characteristics were accomplished through careful addition when Zn^{2+} ions, which preferred tetrahedral locations, were substituted for divalent ions of metal, occupying octahedral sets or preventing grain development (Rehman 2021). The chemical composition of the W-type hexaferrite ($BaNi_2Cr_xFe_{16-x}O_{27}$) was studied by Shi et al. The W-type hexagonal structure exhibits two discernible absorption peaks, each corresponding to the tetrahedral A sites, and the octahedral B sites are visible in the infrared spectrum of the sintered sample (Batoo et al. 2022). Ba-doped Co_Zn ferrite nanoparticles were synthesized using the sol_gel auto-ignition technique. Diffraction X-ray investigation verified that a Single-phase sample with the Fd3m space group was successfully produced. Two prominent peaks in the Fourier-transform infrared (FTIR) spectra, located at approximately 432 cm^{-1} and 583 cm^{-1}, supported the formation of ferrite (Costa et al. 2008). Ni ferrites typically occupy octahedral sites, whereas Zn prefers tetrahedral sites. The interaction between the tetrahedral and octahedral locations influences the electromagnetic properties of the ferrites. Ni^{2+} and Fe^{3+} ions occupy octahedral locations, whereas zinc ions and Fe^{3+} prefer tetrahedral locations. Synthesis methods, sintering temperature, chemical composition, and other factors strongly influence the properties of ferrites (Jain et al. 1981; Sattibabu et al. 2020; Hong 2004). Recent investigations

have indicated that the properties of these ferrites can be improved by the substitution of a small amount of rare-earth cations in the range $0 \leq x \leq 0.25$. The substitution of these cations above a specific concentration generates secondary phases related to $LaFeO_3$, $BaNiO_2$, and NiO2 in addition to hexagonal phase (Ramzan et al. 2019; Ounnunkad et al. 2006).

It is also reported that addition of Ni in small amount ($Ni \leq 0.2$) increases X-ray density of hexaferrites and decreases dislocation density and micro strain in the crystal structure without affecting the lattice parameters (Rafiq et al. 2017). Barium ferrite is a well-known magnetic material with various applications in microwave devices, magnetic recording, and electromagnetic wave absorbers. However, despite its widespread use, there is still a lack of detailed understanding of its optical properties, particularly the refractive index, absorption coefficient, and reflectance. Although some previous studies have investigated the optical properties of barium ferrite using various techniques, there is still a need for more comprehensive and accurate measurements of these parameters, especially in the infrared spectral range. Therefore, there is a research gap in the understanding of the optical properties of barium ferrite, which can be addressed by using advanced spectroscopic techniques such as Fourier transform infrared (FTIR) spectroscopy.

2 Study description

In this study, we examined how the optical properties of $BaNi_{2-x}Zn_xFe_{16}O_{27}$ ferrite are influenced by the introduction of zinc doping by, employing infrared spectroscopy as the analytical tool. We examined the samples of hexagonal ferrites using Fourier-transform infrared (FTIR) analysis, where x varied from 0.0 to 2.0 with a step size of 0.4. A ceramic process was used to create the ferrites.

Our objective was to determine the spectral dependance of the refractive index, absorption coefficient, and reflectance of doped ferrite. These parameters plays a vital role in understanding the optical properties of a material and, are essential for the design and optimization of devices using this material. By examining the infrared transformation, we aimed to gain insights into the optical behavior of $BaNi_{2-x}Zn_xFe_{16}O_{27}$ ferrite and contribute to the advancement of material-based device technologies.

3 Materials and methods

The Zn-doped $BaNi_{2-x}Zn_xFe_{16}O_{27}$ ferrite samples were prepared using the usual Ceramic method. The ceramic method, which is well-established (Al-Hammadi and Khoreem 2022; Khoreem and AL-Hammadi, 2023a, b), and shown in Fig. 1, was utilized to prepare the samples. High-purity $BaCo_3$, ZnO, NiO, and Fe_2O_3 with a purity exceeding 99% were mixed in accordance with their molecular weight ratios to achieve different compositions. The compositions followed the relation $BaCo_3 + (2\text{-}x)(NiO) + x(ZnO) + 8Fe_2O_3 \text{—>} BaNi_{(2-x)}Zn_xFe_{16}O_{27} + CO_2\uparrow$, where x ranged from 0.0 to 2. The weights of the mixed oxides in grams were determined for each composition of the $BaNi_{2-x}Zn_xFe_{16}O_{27}$ system. The oxide mixture was thoroughly ground well using an agate grinder for four hours per sample. The resulting powder mixture was pre-sintered in air at 950 °C ± 10 °C for 6 h, gradually cooled to room temperature. Subsequently, the mixture was ground again for three hours using the mechanical grinding machine to obtain a very fine powder. Finally, the powder was sintered at 1250 °C ± 10 °C for 6 h and slowly cooled to room temperature. The structural

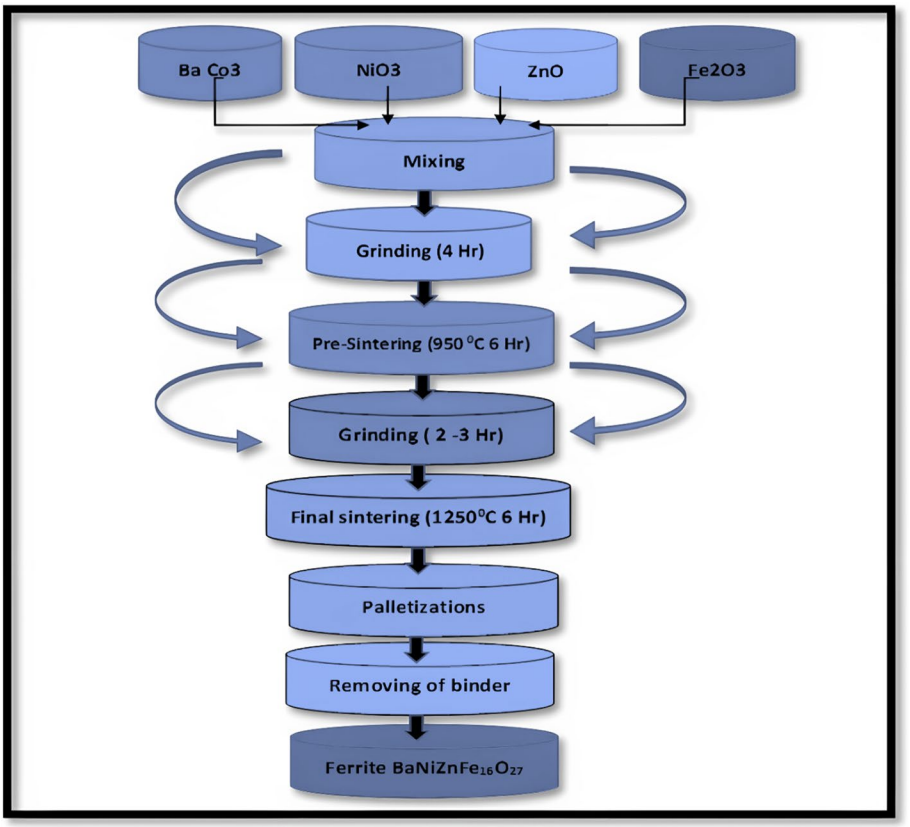

Fig. 1 Schematic diagram outlining the key steps involved in the sample preparation process

properties of the synthesized samples were analyzed using X-ray diffraction (XRD) and Fourier transform infrared spectroscopy (FTIR).

The samples' infrared spectra were measured within the frequency range of 400 and 4000 cm^{-1}, and the optical constants were determined in the frequency range of the quadrupole and octuplet vibration modes in the frit structure. Infrared (IR) radiation absorption spectra were recorded for each of the prepared samples using a Jasco FT/IR-460 PLUS spectrometer located at the Chemistry Department of the Faculty of Science at Sana'a University. The instrument operated in the range of 400–4000 cm^{-1}. The optical constants were determined by classifying the frequencies of the components of the crystal lattice located in the range of 200–4000 cm^{-1} into frequencies of chemical bonds, carriers, and plasma (Caldow et al. 1960). Here, we will study the vibrational sites of the crystal lattice of the compound through IR spectroscopy because the compound has high specific resistance,therefore, the possibility of carriers and plasma frequencies is not available.

Samples were prepared using the Stimson _ Schiedt technique (Caldow et al. 1960). In this process, 0.002 g of powdered sample material was combined with 0.8 mg of bromide (potassium bromide). The blend was introduced into a cylindrical die measuring 20 mm in diameter. Pressure was applied at a rate of 14 tons/cm^2 for approximately 10 min to achieve

compression. This compression resulted in a uniform thickness of the samples, and a small amount of potassium bromide was added to ensure good transparency for IR measurement analysis.

Fourier transform infrared (FTIR) spectra were acquired for all finely powdered samples. The experiments were conducted under ambient conditions and covered 400 to 4000 cm^{-1}, which is the typical range for infrared spectroscopy analysis.

4 Results and discussion

The X-ray diffraction (XRD) analysis revealed that the typical reflections of BaNi2Fe16O27, as represented by the JCPD card (00-54-0097) with the P63/mmc (194) space group, exhibited perfect equivalence to all peaks. This indicates the presence of a well-ordered crystalline structure in the samples. Furthermore, the XRD investigation confirmed the formation of hexagonal W-type single-phase crystalline structures in all examined samples. These findings are consistent with previous studies (Al-Hammadi and Khoreem 2022; Caldow et al. 1960; Khoreem and Al-Hammadi 2023a, b) that have reported similar crystallographic characteristics for $BaNi_2Fe_{16}O_{27}$.

Figure 2 demonstrates a slight leftward shift in all diffraction peaks when Ni is replaced by Zn in the $BaNi_2Fe_{16}O_{27}$ structure. This shift indicates an increase in the interplanar spacing (d) of the crystal lattice, which in turn corresponds to an increase in the lattice parameters a and c. This observation is in agreement with Bragg's formula, which describes the relationship between the diffraction angle (θ), the interplanar spacing (d), the wavelength of X-rays (λ), and the order of the diffraction (n). The leftward shift of the peaks observed in our study suggests that the substitution of Ni with Zn results in an expansion of the crystal lattice.

The determination of the relevant lattice parameters (a and c) was accomplished using XRD analysis, employing equations and Miller indices (hkl). The results showed that as the Zn concentration increased from 0.0 to 2.0, there was an increase in the lattice parameter values, as presented in Table 1. This behavior can be explained by considering the ionic radii of the substituted ions and their respective amounts in the composition. In our case, the larger ionic radius of Zn^{2+} ions (0.74 Å) compared to Ni^{2+} ions (0.68 Å) led to an expansion of the crystal lattice and an increase in the lattice parameters. Similar observations have been reported in previous studies (Al-Hammadi and Khoreem 2022; Caldow et al. 1960; Khoreem and Al-Hammadi 2023a, b), further supporting our findings.

The changes in the lattice parameters and unit cell volume resulting from the substitution of ions can be explained by Vagurd's law, which states that the lattice constant varies linearly with the ionic radii of the substituting ions. In our study, the substitution of Ni with Zn caused an increase in the lattice parameters, consistent with Vagurd's law and the evidence provided by Caldow et al. (Khoreem and Al-Hammadi 2023a, b). This suggests that the rise in lattice parameters is a constant trend governed by the ionic radii of the replacing ions. The average crystallite size for each composition has been calculated from the line broadening of the most intense peak of the magnetoplumbite structure using the classical Scherrer relationship (Jauhar et al. 2012).

$$D_{h\,k\,l} = 0.9\lambda / B\ \cos\theta.$$

where $D_{h\,k\,l}$ is the particle diameter, B is the half maximum line width, λ is wavelength of the radiation used and θ is the angle of diffraction. The crystallite size is found to be in the range of 35–37 nm.

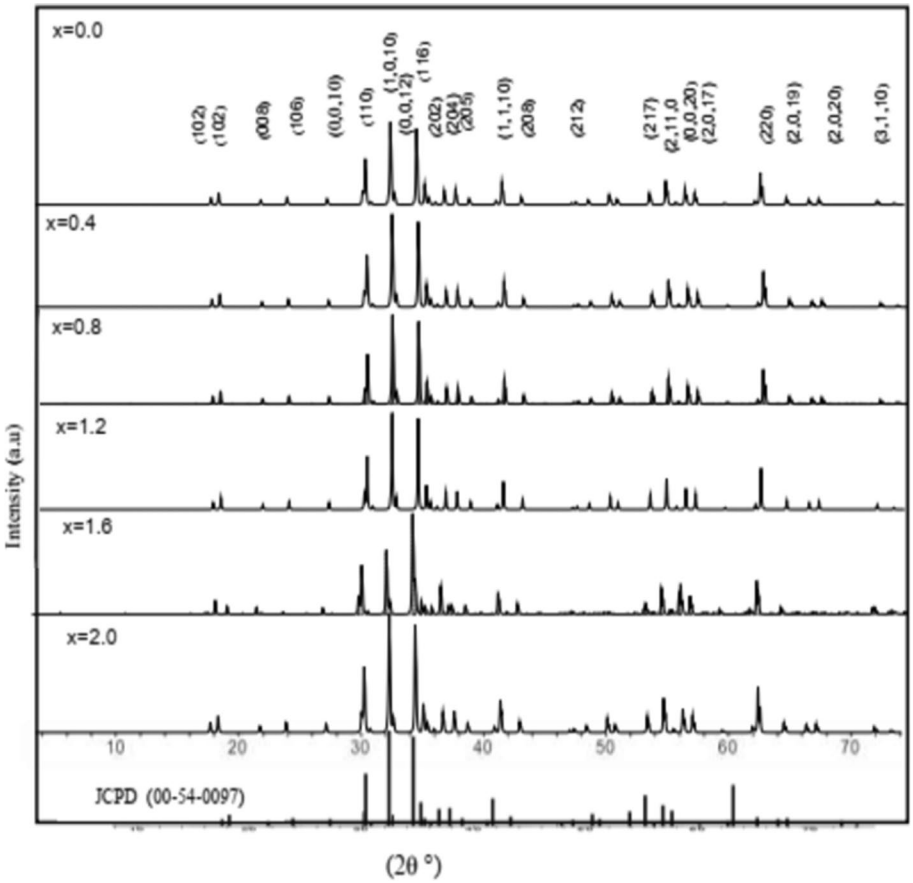

Fig. 2 XRD pattern of $BaNi_{2-x}Zn_xFe_{16}O_{27}$ (x = 0.0, 0.4, 0.8, 1.2, 1.6, and 2) with 2theta (degree) JCPD card (00–54-0097)

Table 1 Microstructure constant (grain size, lattice constant, density, and volume)

Zn	D (nm)	c (Å)	a (Å)	c/a	ρ (g/cm^3)	V (Å^3)
0	35.181	32.734	5.975	5.47849	4.18957	1036.10227
0.4	35.531	32.737	5.976	5.478078	4.27943	1036.5441
0.8	35.814	32.759	5.978	5.47992	4.41655	1037.93507
1.2	36.376	32.784	5.98	5.48227	4.51472	1039.42231
1.6	36.501	32.877	5.981	5.49690	4.55661	1042.71954
2	36.664	32.899	5.997	5.49790	4.62554	1049.00733

Furthermore, the formation of the W-type hexagonal structure in $BaNi_2Fe_{16}O_{27}$ can be recognized when its hexagonal lattice parameters c/a fall within the range of 5.33 to 5.55, as reported in previous studies (Khoreem and Al-Hammadi 2023a, b; Khoreem et al. 2023a, b). In our samples, the value of c/a falls within this range, as shown in Table 1, providing evidence that the W-type hexagonal structure has indeed formed.

In summary, the XRD analysis confirmed the presence of well-defined hexagonal W-type single-phase crystalline structures in $BaNi_2Fe_{16}O_{27}$ samples. The substitution of Ni with Zn resulted in a leftward shift of the diffraction peaks, indicating an increase in the lattice parameters a and c. The increase in lattice parameters can be attributed to the substitution of higher-ionic-radius Zn^{2+} ions for lower-ionic-radius Ni^{2+} ions, leading to an expansion of the crystal lattice. The observed behavior aligns with Vagurd's law and previous studies. Additionally, the c/a values falling within the accepted range further support the formation of the W-type hexagonal structure in our samples. These findings contribute to our understanding of the structural properties of $BaNi_2Fe_{16}O_{27}$ and have implications for its potential applications in nanotechnology.

The XRD data is used to estimate the unit cell volume, V, using the relation, $V = 0.8666*a^2\ c$ (Jauhar et al. 2012) and the values are listed in Table 1.

The investigation of the relationship between structure and the electromagnetic response of ferromagnetic semiconductors has provided valuable insights into their properties (Khoreem and AL-Hammadi 2023a, b). Since the transport and magnetic properties of these materials are strongly influenced by the precise arrangement of atoms or ions within their structures, non-destructive analysis methods are well-suited for studying these properties. Specifically, the spectra of vibrational, electronic, and magnetic dipole modes can provide information about the positions and valences of ions in the crystal lattices.

Among the various analytical techniques available, infrared (IR) spectroscopy is particularly powerful as it enables chemical identification. This technique is based on the principle that chemical substances exhibit selective absorption in the infrared region. Upon absorbing IR radiation, the molecules of the substance vibrate at different rates, resulting in distinct absorption bands known as the "IR absorption spectrum." These bands cover a broad range of wavelengths and correspond to specific functional groups and bonds present in the chemical substance. Therefore, an IR spectrum serves as a unique identifier, especially for organic compounds..

In this study, infrared (IR) absorption spectra were obtained under ambient conditions from 400 to 4000 cm^{-1}. Figure 1 shows the IR spectrum of the as-prepared sample. Notably, two large absorption bands were observed at 1000 cm^{-1}, which is a typical property of ferrites. These bands indicate the formation of hexagonal ferrites. The formation of the structures; $BaNi_{2-x}Zn_xFe_{16}O_{27}$ was proved by FT-IR spectra plotted in the range 400–4000 cm^{-1}. The characteristic FT-IR peaks of our hexaferrite system were found between 438 and 598 cm^{-1} (v_1, and v_2). This result is confirmed with several results were obtained with several published data in hexaferrite studies. (Baleidy et al. 2021; Mosleh et al. 2015).

The stretching vibrations associated with the metal–oxygen bonds produced notably significant peaks at 440 cm^{-1} and 589 cm^{-1}. The frequency range of 550—580 cm^{-1} corresponds to the stretching vibration of the bond between the tetrahedral metal and oxygen ions.

On the other hand, the band observed between 430 and 470 cm^{-1} is due to the connection between the vibrating oxygen ions and the octahedral metallic ions. (Khoreem et al. 2023a, b). Consequently, the bands between 430 to 483 cm^{-1} and 550 and 590 cm^{-1} may be related to the resonance of the octahedral and tetrahedral ferric crystalline sites, respectively (Song et al. 2010).

4.1 Determination of the threshold frequency and threshold energy

Determining the peak of the absorption spectrum can help estimate the threshold frequency (v_{th}) for electronic transitions (Waldron 1955). Upon thorough analysis of the IR spectrum, a low-frequency shoulder (v_{th}) is observed in the composition with x = 0.0, and it occurs at approximately 757 cm^{-1}. This low-frequency shoulder gradually increased and reached its maximum value for the composition with x = 2.0, at approximately 813 cm^{-1} (Fig. 3).

The different masses of the ions that appear at the tetrasite of the hexagonal parameter are responsible for the high-frequency shoulders in the frequency spectrum (Waldron 1955). The discrepancy in mass widens in the current structure as Zn^{2+} replacement occurs, occupying the site. Consequently, the magnitude of the intensity observed in the high-frequency shoulder increased as the Zn content (x) increased. As a result, for the mixture with x = 0.0, the high-frequency shoulder (v_{th}) was 757 cm^{-1}, whereas for the sample with x = 2.0, it was measured 813 cm^{-1} as shown in Table 2.

According to Waldron et al. (Waldron 1955), the saturation point observed at the maximum of the absorption spectra, as depicted in Fig. 3.can serve as a reference for estimating the threshold frequency (v_{th}) for an electronic transition. The point of inflection in the transmittance versus wavenumber graph can be identified as the threshold frequency (v_{th}) for electronic transition. The cutoff frequencies of the $BaNi_{2-x}Zn_xFe_{16}O_{27}$ ferrite system are depicted in (Table 2). It was found that as the zinc content (x) in the system increased, so did the frequency of the electronic transition threshold. The following relationship can be used to determine the relevant threshold energy, and the results are shown in Table 2.

$$E_{th} = h \bullet f = \frac{h \bullet c}{\lambda} = h \bullet c \bullet \nu_{th} \tag{1}$$

As the Zn ion content increased, the threshold frequency (v_{th}) for electronic conversion shifted toward the higher frequency side. resulting in an increase in the corresponding threshold energy (E_{th}), as listed in Table 2. The determined v_{th} and E_{th} values align with those previously reported for mixed Ni– Zn ferrite (Waldron 1955) and $Ni_{0.5}Zn_{0.5}Fe_2O_4$ ferrite (Modi et al. 2013).

It is worth highlighting that both the v_{th} and Eth values exhibit consistency with the reported values for mixed Ni–Zn ferrite and are subject to significant uncertainty because it is challenging to distinguish the scattering from the absorption losses caused by ferrite particles. The measured values can be embodied as activation energy values if the measured absorption corresponds to the transition to a conduction band in the vicinity of the crystal (Waldron 1955).

Table 2 Threshold energy (E_{th}) and infrared absorption frequency (υ) for $BaNi_{2-x}Zn_xFe_{16}O_{27}$ system at room temperature

Zn content (x)	ν_1 cm^{-1}	ν_2	ν_{th}	E_{th} (ev)
Zn = 0	595.896	432.94	757.89	0.0939
Zn = 0.4	590.111	433.905	763.7	0.0946
Zn = 0.8	583.361	434.834	804.17	0.09963
Zn = 1.2	584.325	435.834	808.3	0.10014
Zn = 1.6	581.433	438.726	810.92	0.10047
Zn = 2	580.469	439.69	813.31	0.1007

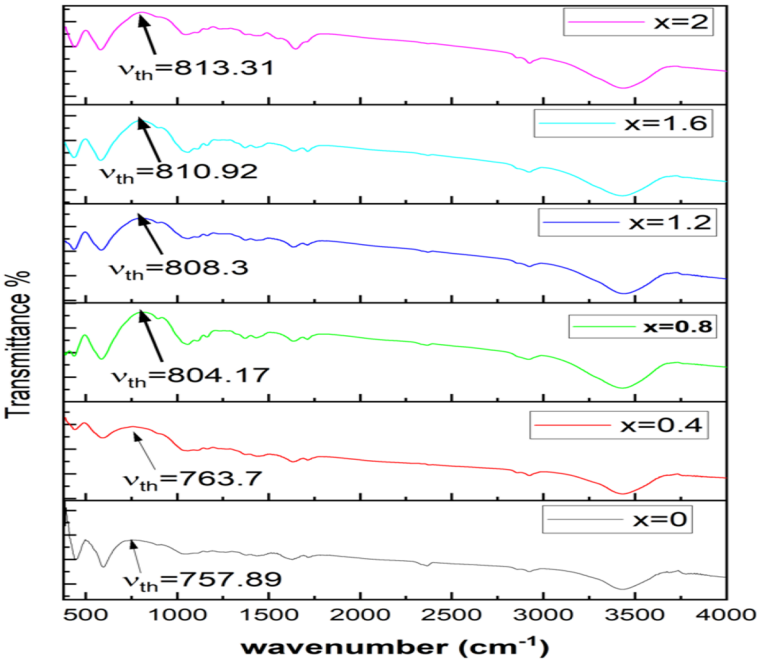

Fig. 3 Variation of the absorption spectra and v_{th} with wave numbers

4.2 Optical parameter determination

When electromagnetic radiation interacts with materials, it is often crucial to know their optical properties to predict and manipulate their responses. Understanding the underlying mechanisms responsible for their optical behavior enables us to make informed predictions. The equation provided in references (Hemada 2004; Kittel 1976), can be used to approximate the refractive index (η) and velocity (v) of infrared light in a ferrite material. By employing the values of transmission energy (Eth), absorbed energy (Eab), and speed of light (c), it is possible to compute the index of refraction (η) and velocity (v) of infrared radiation in the ferrite material. The calculation can be performed using the following equation:

$$\eta = c / v = E_{th}/E_{ab} \tag{2}$$

$$\frac{E_t}{E_{ab}} = \frac{c}{n} = \eta \tag{3}$$

This equation allows the estimation of the index of refraction (η) and velocity (v) of infrared radiation in a given ferrite material, given the values of transmitted energy (E_{th}) and absorbed energy (Eab). The velocity of light (c) is a constant.

The magnitude of the refractive index (η), which determines the degree of light bending, is affected by the wavelength of the incident radiation. In general, the refractive index decreases as the wavelength increases (Johnson and Walton 1965). In this scenario, the wavelengths (1 and 2) that correlate with the positions of the main infrared

absorption bands (v_1 and v_2) were considered while calculating the values of the refractive index (η_1 and η_2). The average refractive index (η_{ave}) was then determined on the basis of these values. Subsequently, for various compositions, the mean refractive index was employed to determine the velocity (v), reflectivity (R), and jump rate (J).

When comparing the obtained values depicted in Table 3, it is evident that as the Zn concentration (x) inside the ferrite composition increase, the value of the refractive index ($\boldsymbol{\eta}_{ave}$) increases, while the velocity (v) of the infrared radiation drops. These findings indicate a relationship between the composition of a material and its optical properties.

In the investigated system $BaNi_{2-x}Zn_xFe_{16}O_{27}$, the retardation or slowing of infrared radiation in a medium is primarily caused by electronic polarization. The extent of this effect is significantly influenced by the size of the atoms or ions constituting the medium. In general, larger atoms or ions result in greater electronic polarization, leading to a slower velocity of light propagation and a higher refractive index.

For instance, when large ions, such as barium ions or lead ions, are added to the glass material, the refractive index values increase. Highly leaded glasses, which contain a high weight percentage (90 wt%) of PbO, have an approximate refractive index of 2.1. This demonstrates the substantial impact of large ions on the optical characteristics of the materials (Callister 2000).

In $BaNi_{2-x}Zn_xFe_{16}O_{27}$ system, the larger ions of Zn^{2+} (0.74) take the place of the smaller ions of nickel (0.68). It is expected that the refractive index (η) would increase or remain unaffected, which aligns with the observed trend shown in Table 3. This can be attributed to the crucial role played by Zn, which has a higher refractive index of 1.75 (Callister 2000).

The refractive index values obtained in the $BaNi_{2-x}Zn_xFe_{16}O_{27}$ system are therefore similar to those obtained for magnetic oxides spinel ($MgAl_2O_4$, = 1.72), single crystalline iron garnets, including yttrium iron garnet, gadolinium-yttrium iron garnet, and europium iron garnet with a composition of (2.2–0.2) (Johnson and Walton 1965).The index of refraction ($\boldsymbol{\eta}$) of crystal ceramics with a hexagonal crystal structure, as in this system, is independent of the crystallographic orientation and displays isotropic behavior. However, in non-cubic crystals, the refractive indices are anisotropic, meaning they vary based on the crystallographic direction. The highest refractive index is typically observed along the direction that corresponds to the highest ion density within the crystal structure.

Table 3 Jump rate (J)), velocity (v), reflectivity (R) and refractive index (η) for $BaNi_{2-x}Zn_xFe_{16}O_{27}$ system at room temperature

Zn content (x)	η_1	η_2	η_{av}	R (%)	Velocity(v) (cm/s)*10^8	J_1 (Hz)*10^{12}	J_2	J
Zn = 0	1.2718	1.7505	1.5112	4.144	198.516	1.7806	2.1713	1.9759
Zn = 0.4	1.2941	1.7600	1.5271	4.35	196.449	1.8123	2.1779	1.9951
Zn = 0.8	1.3785	1.8493	1.6139	5.516	185.880	1.9112	2.2163	2.0638
Zn = 1.2	1.3833	1.8546	1.6189	5.585	185.304	1.9133	2.2168	2.0650
Zn = 1.6	1.3946	1.8483	1.6215	5.620	185.011	1.9224	2.2135	2.0680
Zn = 2	1.4011	1.8497	1.6254	5.674	184.566	1.9280	2.2137	2.0708

Regarding the reflectivity of the ferrite materials, an attempt has been made to calculate it using a specific relation.

$$R = \left(\frac{\eta_{ave}-1}{\eta_{ave}+1}\right)^2 \tag{4}$$

The relationship provided states that the reflectivity (R) of a material is influenced by its refractive index (η_{ave}). A higher refractive index leads to greater reflectivity. In the $BaNi_{2-x}Zn_xFe_{16}O_{27}$ system, the reflectivity (R) values exhibit the expected changes. According to the data presented in Table 3, the reflectivity increased from 0.041 for the composition with x = 0.0 to 0.0567 for the composition with x = 2.0.

Charged vacancies may arise to preserve the localized neutrality of charges when an ion with the wrong valence is added to the crystalline structure. Thermoelectric power measurements indicate that all compositions in the $BaNi_{2-x}Zn_xFe_{16}O_{27}$ system exhibit n-type semiconducting behavior, which means that electron conduction predominates. As a result, anion vacancies rather than cation vacancies are more prone to occur as vacancies. This result is supported by the observation that Fe^{2+} ions have a lower valence than Fe^{3+} ions, that anions are more likely to be involved in the vacancy formation process.

The charge carriers' jump frequency (J_1 and J_2) (electrons) of vibration of the tetrahedral and octahedral was calculated, and the average of J_1, and J_2 Finally, used to calculate the jump rate (J) of the charge carriers (in this case, electrons) can be estimated using a specific relation.

$$J = fe^{\frac{-E}{K_B}}T \tag{5}$$

. Based on the relation mentioned, the jump frequency (J) of charge carriers (electrons) in the $BaNi_{2-x}Zn_xFe_{16}O_{27}$ system can be estimated using the vibration frequency (f), The Boltzmann constant (k_B) and the height of the potential barrier (E), which signifies the activation energy for electron hopping, are both factors considered in this context. The jump rate (J) evidently increases when Zn percent (x) increases for $BaNi_{2-x}Zn_xFe_{16}O_{27}$ samples. This increase is due to the higher number of anion vacancies formed because of the presence of ferrous (Fe^{2+}) ions in the lattice. The introduction of Zn leads to the formation of anion vacancies, which provide more available pathways for electron hopping, resulting in an increased jump rate. This finding that Zn content is a key factor in the system's conductivity and mobility of charge carriers.

However, equations are related to the cation distribution and ionic radii for T_d and O_h sites. Unfortunately, you did not provide those equations. The following equations related to the cation distribution and ionic radii in the context of jump rate and charge carrier behavior in the $BaNi_{2-x}Zn_xFe_{16}O_{27}$ system (Potakova et al. 1972; Dawoud et al. 2017).

$$R_T = R_{Ba^{2+}} + xR_{Zn^{2+}} + (2-x)R_{Fe^{3+}} \tag{6}$$

$$R_O = \frac{1}{2}\left[(2-x)R_{Ni^{2+}} + (2+x)R_{Fe^{3+}}\right] \tag{7}$$

In the $BaNi_{2-x}Zn_xFe_{16}O_{27}$ system, the cation distribution and their corresponding ionic radii play a role in determining the behavior of the system based on the given data:

- R_{Ba2+} indicates the Ba ion's ionic radius.
- R_{Zn2+} indicates the Zn ion's ionic radius.

– R_{Fe2+} represents the iron ion radius.
– R_{Ni2+} represents the nickel ion radius.

In the system, the average ionic radii per molecule for the tetrahedral (T_d) site is represented as R_T, while R_O stands for the average radii of ions per molecule for the octahedral (O_h) site.

It is observed that as the Zn^{2+} ions increase in the system. The average ionic radii at the molecule for the tetrahedral site (R_T) value rises. This effect is explained by the addition of Zn ions to the tetrahedral sites for Fe ions, which typically have a higher ionic radius. On the other hand, as the amount of Zn^{2+} ions increases, the value of R_O (the average ionic radii per molecule for the octahedral site) decreases. The replacement of Ni ions, which caused this drop, which generally have a smaller ionic radius than Fe ions, with Zn ions to the octahedral sites.

These observations that the addition of zinc ions in the $BaNi_{2-x}Zn_xFe_{16}O_{27}$ system affects the mean ionic radii at both the tetrahedral and octahedral sites, leading to changes in the crystal structure and potentially influencing the material's properties.

The reduction in R_O can be attributed to a decline in the quantity of Ni^{2+} ions occupying the B-site, because they possess larger ionic radii. In contrast, the increase in RT is the result of more zinc ions—which have a greater ionic radius of approximately 0.74 and a smaller one of approximately 0.67—replacing smaller Fe^{3+} ions on the tetrahedral (A-site).

Table 4, and Fig. 4, is explained contains the cation distribution, calculated ionic radii for R_T and R_O, and the R_T/R_O ratio. Where R_T and R_O are the mean ionic radii per molecule for tetrahedral T_h and octahedral O_h sites, respectively.

5 Conclusion

1. The powder X-ray diffraction studies confirmed the formation of W-type hexaferrite structure. XRD results were used to determine the crystallite size and lattice constants of the prepared powders. The average crystallite size was found in the range of 35–37 nm and increased with increase in Zn^{2+} content.
2. Infrared (IR) spectra analysis of the $BaNi_{2-x}Zn_xFe_{16}O_{27}$ ferrites revealed two main bands. One band is associated with the vibrations occurring at the tetrahedral site around 598 cm^{-1}, while the other band corresponds to the vibrations at the octahedral site

Table 4 Values of R_T, R_O, and R_T/R_O for $BaNi_{2-x}Zn_xFe_{16}O_{27}$ ferrite

X	Cation distribution	R_T (nm)	R_O (nm)	R_T/R_O
0.0	$\left(Ba^{2+}Zn^{2+}_{0.0}Fe^{3+}_{8.0}\right)\{Ni^{2+}_{2.0}Fe^{3+}_{8.0}\}O^{2-}_{27}$	*0.262*	*0.133*	1.969
0.4	$\left(Ba^{2+}Zn^{2+}_{0.4}Fe^{3+}_{7.6}\right)\{Ni^{2+}_{1.6}Fe^{3+}_{8.4}\}O^{2-}_{27}$	*0.266*	*0.132*	2.015
0.8	$\left(Ba^{2+}Zn^{2+}_{0.8}Fe^{3+}_{7.2}\right)\{Ni^{2+}_{1.2}Fe^{3+}_{8.8}\}O^{2-}_{27}$	*0.27*	*0.131*	2.061
1.2	$\left(Ba^{2+}Zn^{2+}_{1.2}Fe^{3+}_{6.8}\right)\{Ni^{2+}_{0.8}Fe^{3+}_{9.2}\}O^{2-}_{27}$	*0.274*	*0.13*	2.107
1.6	$\left(Ba^{2+}Zn^{2+}_{1.6}Fe^{3+}_{6.4}\right)\{Ni^{2+}_{0.4}Fe^{3+}_{9.6}\}O^{2-}_{27}$	*0.278*	*0.129*	2.155
2	$\left(Ba^{2+}Zn^{2+}_{2.0}Fe^{3+}_{6.0}\right)\{Ni^{2+}_{0.0}Fe^{3+}_{10.0}\}O^{2-}_{27}$	*0.282*	*0.128*	2.203

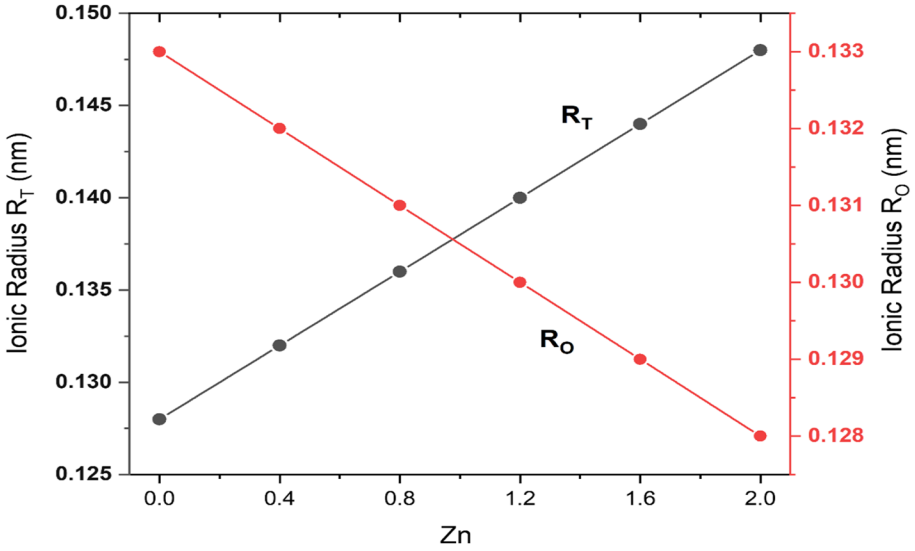

Fig. 4 Variation of R_T and R_O with the Zn ratio" s"

around 443 cm^{-1}. These bands represent specific vibrational modes within the ferrite crystal structure.

3. The threshold frequency and energy of the electronic transitions in the ferrite material were determined. This information provides insights into the electronic properties and behavior of the material.
4. Numerous significant optical properties can be determined by infrared spectral analysis. In the $BaNi_{2-x}Zn_xFe_{16}O_{27}$ system, these metrics may include the index of refraction, reflectivity, and jump rate, all of which are observed to display distinct trends with increasing Zn substitution.
5. As Zn substitution rises, it is noticed that the velocity of infrared radiation in the given ferrite material decreases. This decrease in velocity can be attributed to the influence of Zn ions, which have a larger size than the original Ni ions. The presence of larger ions results in a slower propagation of the infrared radiation through the material.
6. It is discovered that as Zn substitution increases, the refractive index, reflectivity, and jump rate all rise. This increase is likely due to the larger size of the Zn ions, which leads to enhanced electronic polarization and greater optical reflectivity. The presence of Zn ions also contributes to the formation of anion vacancies, which promote the movement of charge carriers (such as electrons) and increase the jump rate of these carriers within the ferrite material.
7. By analyzing the IR absorption bands, estimations of the cation distributions within the $BaNi_{2-x}Zn_xFe_{16}O_{27}$ ferrites can be made. The observed vibrational frequencies and their assignments provide insights into the arrangement and distribution of different cations (such as Zn, Fe, and Ni) across the tetrahedral and octahedral sites of the ferrite structure.

These conclusions highlight the significance of IR spectral analysis in understanding the structural, optical, and electronic properties of $BaNi_{2-x}Zn_xFe_{16}O_{27}$ ferrites, particularly in relation to Zn substitution.

Supplementary Information The online version contains supplementary material available at https://doi.org/10.1007/s11082-023-06050-7.

Acknowledgements The authors appreciate the contribution of the reviewers in improving the quality of this paper. The authors are grateful to the head of the Physics Department at the Faculty of Sciences, Sana'a University, Yemen. The authors are thankful to the FT-IR laboratory team in the Chemistry Department for providing their laboratory to carry out the present work. (Research assistant: Munther AL-Hakymy).

Author contributions 1,2;3:wrote the main manuscript text and. prepared figures. All authors reviewed the manuscript."

Funding The authors declare that no funds, grants, or other support were received during the preparation of this manuscript.

Data availability The datasets used and/or analysed during the current study are available from the corresponding author on reasonable request**.**

Declarations

Conflict of interest We declare that the authors have no competing interests as defined by Springer, or other interests that might be perceived to influence the results and/or discussion reported in this paper. I declare that the authors have no competing interests as defined by Springer, or other interests that might be perceived to influence the results and/or discussion reported in this paper.

Ethical approval This work is not applicable for both human and/ or animal studies.

References

Al-Hammadi, A.H., Khoreem, S.H.: Investigations on optical and electrical conductivity of Ba/Ni/Zn/$Fe_{16}O_{27}$ ferrite nanoparticles. Biointerface Res. Appl. Chem. **13**(2), 168 (2022)

Baleidy, W.S., et al.: Impact of rare-earth ions on the physical properties of hexaferrites $Ba_{0.5}Sr_{0.5}RE_{0.6}Fe_{11.4}O_{19}$, (RE = La, Yb, Sm, Gd, Er, Eu, and Dy). J. Alloys Compd. **873**, 159812 (2021). https://doi.org/10.1016/j.jallcom.2021.159812

Batoo, K., Hadi, M., Verma, R., Chauhan, A., Kumar, R., Singh, M., Aldossary, O.: Improved microwave absorption and EMI shielding properties of Ba-doped Co–Zn ferrite. Ceram. Int. **4**, 3328–3334 (2022)

Bharati, V., Somvanshi, S., Humbe, A., Murumkar, V., Sondur, V., Jadhav, K.: Influence of trivalent Al–Cr co-substitution on the structural, morphological and Mössbauer properties of nickel ferrite nanoparticles. J. Alloys Compd. **821**, 153501 (2020)

Caldow, G.L., Van Cleave, A.B., Eager, R.L.: The infrared spectra of some uranyl compounds. Can. J. Chem. **38**(6), 772–782 (1960)

Callister, W. D.: Materials Science and Engineering An-Introduction (2000)

Costa, A., Silva, V., Cornejo, D., Morelli, M., Kiminami, R., Gama, L.: Magnetic and structural properties of $NiFe_2O_4$ ferrite nanopowder doped with Zn^{2+}. J. Magn. Magn. Mater. **320**, e370–e372 (2008)

Dawoud, H., OUDA, L., Shaat, S.K.K.: FT-IR studies of nickel substituted polycrystalline zinc spinel ferrites for structural and vibrational investigations. Chem. Sci. Trans. **6**, 179–188 (2017)

Dhiman, P., Jasrotia, R., Goyal, D., Mola, G.T.: Hexagonal ferrites, synthesis, properties and their applications. Mater. Res. Found **112**, 336–370 (2021)

Hemada, J.O.H.: IR Spectral studies of $Co_{0.6}Zn_{0.4}Mn_xFe_{2-x}O_4$ Ferrites. J. Magn. Magn. Mater **281**(1), 36–41. https://doi.org/10.1016/j.jmmm.2004.01.100.J

Hong, Y.S., Ho, C.M., Hsu, H.Y., Liu, C.T.: Synthesis of nanocrystalline Ba $(MnTi)_xFe_{12-2x}O_{19}$ powders by the sol–gel combustion method in citrate acid–metal nitrates system (x= 0, 0.5, 1.0, 1.5, 2.0). J. Magn. Magn. Mater. **279**(2–3), 401–410 (2004)

Jain, S., Adiga, K., Pai Verneker, V.: A new approach to thermochemical calculations of condensed fuel-oxidizer mixtures. Combust. Flame **40**, 71–79 (1981)

Jauhar, S., et al.: Structural, morphological, magnetic and optical properties of chromium substituted strontium ferrites, $SrCr_xFe_{12-x}O_{19}$ (x = 0.5, 1.0, 1.5, 2.0 and 2.5) annealed with potassium halides. Powder Technol. **212**(211), 193–197 (2012). https://doi.org/10.1016/j.powtec.2011.05.014

Johnson, B.B., Walton, A.K.: The infra-red refractive index of garnet ferrites. Br. J. Appl. Phys. **16**(4), 475–477. https://doi.org/10.1088/0508-3443/16/4/310

Khoreem, S.H., Al-Hammadi, A.H.: Synthesis and unveiling the effect of nonmagnetic Zn^{2+} ions on enrichment of structural properties of barium-nickel ferrites. Biointerface Res. Appl. Chem. **13**(5), 488 (2023a)

Khoreem, S.H., AL-Hammadi, A.H.: Effect of nonmagnetic doping on dielectric properties and initial permeability of Ba–Ni ferrite nanoparticles by virtue of Zn^{2+} ions. Adv. Mater. Sci. Eng. **2023**, 1–10 (2023b). https://doi.org/10.1155/2023/5586664

Khoreem, S.H., et al.: Investigation of Zn substituted Ba-W-type base ferrites for FT-IR structural and vibrational studies. Lett. Appl. Nanobiosci. **12**(4), 164 (2023a)

Khoreem, S.H., et al.: Effect of nonmagnetic doping on dielectric properties and initial permeability of Ba–Ni ferrite nanoparticles by virtue of Zn^{2+} ions. Adv. Mater. Sci. Eng. **2023**, 1–10, Article ID 5586664 (2023b)

Kittel, C.: Introduction to Solid State Physics, p. 323 (1976)

Kulkarni, A., Mathad, S.: Effect of cadmium doping on structural and magnetic studies of Co–Ni ferrites. Sci. Sinter. **53**, 407–418 (2021)

Modi, K.B., et al.: Infrared spectral evolution, elastic, optical and thermodynamic properties study on mechanically milled $Ni_{0.5}Zn_{0.5}Fe_2O_4$ spinel ferrite. J. Mol. Struct. **1049**, 250–262 (2013)

Mosleh, P., et al.: Structural, magnetic, and microwave absorption properties of Ce-doped barium hexaferrite. J. Mag. Mag. Mater. **397**, 101–107 (2015)

Narang, S.B., Pubby, K.: Nickel spinel ferrites: a review. J. Magn. Magn. Mater. **519**, 167163 (2021). https://doi.org/10.1016/j.jmmm.2020.167163

Ounnunkad, S., et al.: Effect of La doping on structural, magnetic and microstructural properties of $Ba_{1-x}La_xFe_{12}O_{19}$ ceramics prepared by citrate combustion process. J. Electroceram. **16**, 357–361 (2006)

Potakova, V.A., Zverev, N.D., Romanov, V.P.: On the cation distribution in $Ni_{1-x-y}Fe\ Zn_yFeO_4$ spinel ferrites. Phys. Status Solidi (a) **12**(2), 623–627 (1972). https://doi.org/10.1002/pssa.2210120235

Rafiq, M.A., et al.: Effect of Ni^{2+} substitution on the structural, magnetic, and dielectric properties of barium hexagonal ferrites ($BaFe_{12}O_{19}$). J. Electron. Mater. **46**, 241–246 (2017)

Ramzan, M., et al.: Effect of La and Ce co-doping on structural, spectral and electrical properties of Ba–Ni M type hexaferrites. Dig. J. Nanomater. Biostruct. **14**, 849–854 (2019)

Rehman, A.: Synthesis and investigations of structural, magnetic and dielectric properties of Cr-substituted W-type Hexaferrites for high frequency applications. J. Electroceram. **46**, 93–106 (2021)

Sattibabu, B., Rao, T., Das, T., Chatterjee, M., Bhatnagar, A., Rayaprol, S., Das, D.: Synthesis and magnetic properties of nanostructured $Ni_{1-x}Zn_xFe_2O_4$ (x = 0.4, 0.5 and 0.6). In: AIP Conference Proceedings (2020)

Song, F., et al.: Formation and magnetic properties of M-Sr ferrite hollow fibers via organic gel-precursor transformation process. Mater. Chem. Phys. **120**(1), 213–216 (2010)

Waldron, R.D.: Infrared spectra of ferrites. Phys. Rev. **99**(6), 1727–1735 (1955)

Authors and Affiliations

Sadiq H. Khoreem[1] · A. H. AL-Hammadi[2] · Azmi A. M. Othman[3]

✉ Sadiq H. Khoreem
khoreems@yahoo.com

A. H. AL-Hammadi
hkm_hammadi@yahoo.com

Azmi A. M. Othman
azmihameed@yahoo.com

[1] Department of Optometry and Vision Science, Faculty of Medical Science, Al-Razi University, Sana′a, Yemen

[2] Physics Department, Faculty of Science, Sana′a University, Sana′a, Yemen

[3] Yemen Standardization, Metrology, and Quality Control Organization, Sana′a, Yemen